



Mechanistic Insights into EGFR Membrane Clustering Revealed by Super-resolution Imaging

Journal:	<i>Nanoscale</i>
Manuscript ID:	NR-ART-08-2014-004962.R2
Article Type:	Paper
Date Submitted by the Author:	08-Dec-2014
Complete List of Authors:	<p>Wang, Hongda; Changchun Institute of Applied Chemistry, State Key Laboratory of Electroanalytical Chemistry gao, jing; Changchun Institute of Applied Chemistry, Chinese Academy of Sciences, State Key Laboratory of Electroanalytical Chemistry Wang, Ye; Institute of Biochemistry and Cell Biology, Shanghai Institutes for Biological Sciences, State Key laboratory of Cell Biology Cai, Mingjun; Changchun Institute of Applied Chemistry, Chinese Academy of Sciences, State Key Laboratory of Electroanalytical Chemistry Pan, Yangang; Changchun Institute of Applied Chemistry, State Key Laboratory of Electroanalytical Chemistry, Xu, Haijiao; Changchun Institute of Applied Chemistry, Chinese Academy of Sciences, State Key Laboratory of Electroanalytical Chemistry Jiang, Junguang; Changchun Institute of Applied Chemistry, State Key Laboratory of Electroanalytical Chemistry, Ji, Hongbin; Institute of Biochemistry and Cell Biology, Shanghai Institutes for Biological Sciences, State Key laboratory of Cell Biology</p>

Cite this: DOI: 10.1039/c0xx00000x

www.rsc.org/xxxxxx

ARTICLE TYPE

Mechanistic Insights into EGFR Membrane Clustering Revealed by Super-resolution Imaging

Jing Gao^{a,c}, Ye Wang^b, Mingjun Cai^a, Yangang Pan^{a,c}, Haijiao Xu^a, Junguang Jiang^a, Hongbin Ji^{*b} and Hongda Wang^{*a}

5 Received (in XXX, XXX) Xth XXXXXXXXXX 20XX, Accepted Xth XXXXXXXXXX 20XX

DOI: 10.1039/b000000x

The clustering of membrane receptors such as EGFR is critical for various biological processes, for example, cell signaling and tumorigenesis. However, the mechanism involved remains poorly understood. Here, we used a super resolution imaging technique, which has shattered the longstanding resolution barrier of light diffraction, to investigate the distribution of membrane EGFR on apical or basal surfaces of COS-7 cells and on the surface of suspension COS-7 cells. Our data show that more and larger EGFR clusters are detected on the apical surface in comparison with those on the basal surface and this difference is not affected by EGFR activation status, whereas suspension COS-7 cells exhibit a moderate clustering status and a homogenous distribution pattern, indicating the decisive factor of external environment surrounding the cell membrane in EGFR clustering pattern. A dual-color dSTORM imaging reveals the significant colocalization of EGFR and lipid rafts; interestingly M β CD treatment leads to a dramatic decrease of the amount and size of EGFR clusters on both apical and basal surfaces, highlighting a key role of lipid rafts in EGFR cluster formation. Together, our results illustrate the distribution pattern of EGFR in polarized cells and uncover the essential role of lipid rafts in EGFR cluster maintenance.

20 Introduction

The plasma membrane is a complex bilayer system including a variety of special membrane microdomains, for example lipid rafts¹, and diverse membrane proteins. Many studies using conventional fluorescence microscopy and biochemical methods have implied that membrane proteins are not distributed homogeneously in the plasma membrane²⁻⁴. However, due to the diffraction limit of light, fluorescence microscopes were generally unable to detect the precise distribution patterns of the membrane proteins. Fortunately, several super-resolution fluorescence microscopy techniques, such as stochastic optical reconstruction microscopy (STORM)⁵⁻⁶, direct STORM (dSTORM)⁷, photoactivated localization microscopy (PALM)⁸⁻⁹ and stimulated-emission depletion (STED) microscopy¹⁰, have broken the diffraction barrier and offered opportunities to study the protein distribution at the single molecule level¹¹⁻¹². So far, they have revealed a noticeable protein clustering phenomenon, particularly for membrane proteins such as GPI-anchored proteins, T cell antigen receptors and toll-like receptors, and this clustering pattern necessarily regulates their functions¹³⁻¹⁷. It has become increasingly clear that exploring protein distribution pattern on the nanometer scale is vital for deciphering how protein organization links to protein physiological functions.

The epidermal growth factor receptor (EGFR), as a typical receptor tyrosine kinase of the ErbB family, plays a crucial role in regulating cell growth, proliferation and differentiation¹⁸⁻²⁰.

Aberrant activation or over-expression of EGFR is implicated in many tumors²¹. The initial step of EGFR signal transduction is the activation of EGFR by binding of its specific ligands to the extracellular domain, which induces the dimerization and activation of the intracellular kinase domains^{18, 22-23}. The C-terminal tyrosine residues are then phosphorylated, which elicit downstream signal transduction through the recruitment of several related adaptor proteins²⁴. A previous study using the NSOM technique has suggested that EGFR might aggregate and form clusters on the cell surface²⁵. Our recent work has also observed EGFR clusters on the cell membrane²⁶. Nevertheless, some key questions on EGFR clustering remain unsolved and deserve to be further explored. For example, epithelial cells are usually polarized in vivo, with the apical membrane surface facing the outside environment and the basal membrane surface attaching to the basement membrane. Given that many malignant cancers are epithelial-derived, it's interesting and important to test how EGFR proteins are distributed on different membrane surfaces of epithelial cells. Furthermore, considering previous studies have shown the detailed structure of different existing forms of EGFR, such as monomers²⁷, inactive dimers²⁸ and active dimers²⁹, it also attracts our attentions that whether EGF stimulation-induced EGFR activation would affect the distribution of EGFR.

Lipid rafts, as dynamic membrane domains with the size from 10 nm to 200 nm, are consisted of cholesterol, sphingolipids, and some specific proteins, and play an important role in cell signaling and molecule trafficking³⁰⁻³¹. Some studies have

indicated that lipid rafts can regulate the assembly of proteins³¹⁻³². Thus, it would be interesting to study whether lipid rafts are key regulators of EGFR clustering. To answer these questions, studies using a high-resolution microscopy for direct visualization of proteins with nanoscale precision at single molecule level are required.

We here utilized dSTORM for imaging the spatial distribution of EGFR at inactive status or ligand-stimulated active status on different membrane surfaces of COS-7 cells, and further visualizing the relationship of localization between EGFR and lipid rafts. This technique relies on fluorophores that can be switched between a bright on and a dark off state. Each time only a few sparse molecules are randomly excited to bright on state, while other majorities of molecules are in the dark off state. By repeating this process, a series of images can be collected and the positions of individual molecules emerged in every image can be identified. Finally a reconstructed super-resolution image is obtained by accumulating the precise locations of every detected molecule. This novel approach allows direct observation of EGFR distribution in the plasma membrane with a resolution about 30 nm (Fig. S1) and also offers precise spatial association between EGFR and lipid rafts. Thus we are able to measure the number and size of EGFR clusters in different membrane surfaces, as well as the change of EGFR clusters after EGF stimulation. Solving these questions could provide a comprehensive understanding of the molecular mechanism of EGFR activation.

Results and discussion

Super-resolution imaging of inactive EGFR clustering

We first utilized dSTORM for imaging the spatial distribution of inactive EGFR proteins on different membrane surfaces of COS-7 cells: the apical membrane surfaces and the basal membrane surfaces; meanwhile, we suspended the COS-7 cells to deprive their polarity and then observed their membrane surfaces (see Experimental Section for the details of preparing suspension cells). Different surfaces of the cell membrane confront different external environments for membrane receptors. EGFR was labeled with Alexa647-conjugated Cetuximab, an EGFR antibody that can compete with EGFR ligands and block EGFR activation³³, so the EGFR proteins we observed are inactive.

Fig. 1a-c showed the distribution of inactive EGFR on the apical and basal surfaces of adherent COS-7 cells, and on the membrane surface of the suspension COS-7 cell, respectively. EGFR expression levels on different membrane surfaces were estimated by detecting the number of the fluorescent localizations of every reconstructed dSTORM image, which is almost proportionate to the amount of EGFR proteins (Fig. S2). The statistic result of EGFR levels showed that there was no significant difference of EGFR levels on the three types of membrane surfaces. The inactive EGFR proteins are prevalently

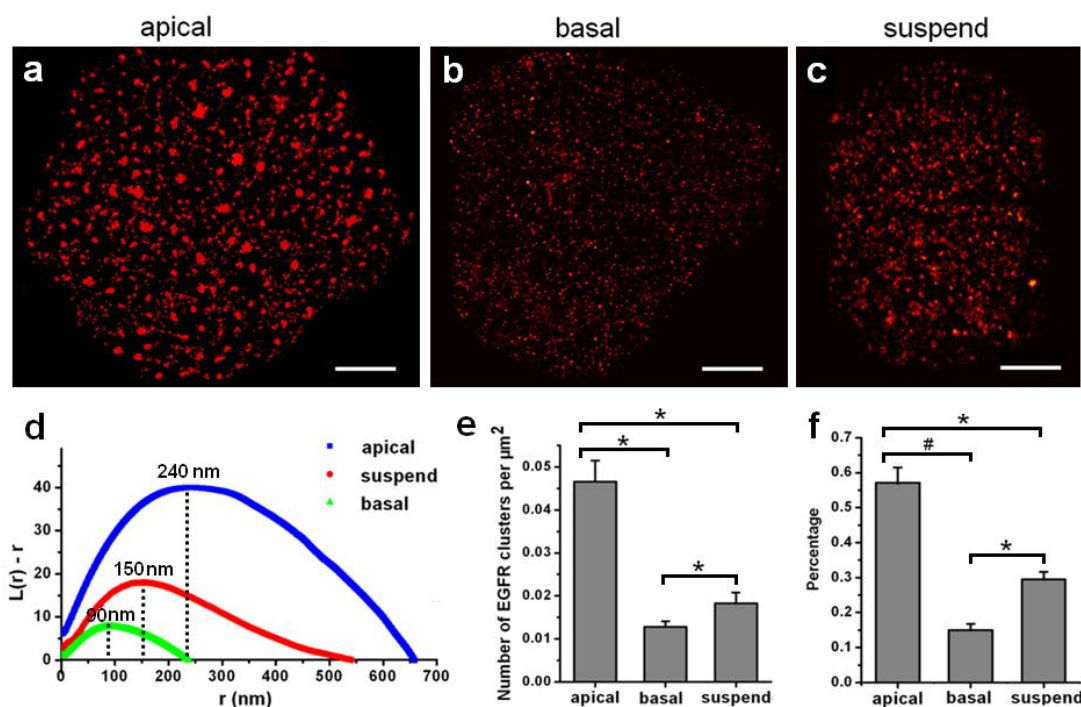


Fig. 1 EGFR proteins at inactive status form clusters with different number and size on different membrane surfaces of adherent COS-7 cells and suspension cells. (a-c) Typical reconstructed dSTORM images of inactive EGFR on the apical surface of the adherent COS-7 cell (a), on the basal surface of the adherent COS-7 cell (b) and in the membrane of the suspension COS-7 cell (c), respectively. EGFR was labeled with Alexa647-conjugated Cetuximab. Scale bars indicate 10 μm. (d) Representative Ripley's K function analysis of EGFR clustering on the different membranes. The analysis is applied to the stochastic regions of $2 \times 2 \mu\text{m}^2$ in the reconstructed images. The values of r_{max} are 240 nm, 90 nm and 150 nm on the apical surface, basal surface of the adherent cell and in the membrane of the suspension cell, respectively. 60 regions from 10 cells in 5 independent experiments are analyzed and obtained nearly the same results. (e) Normalized average number of EGFR clusters per μm^2 under the different conditions. (f) The percentage of EGFR forming clusters under the different conditions. Data in (e) and (f) are the means \pm standard deviation (s.d.), which were obtained from 10 cell samples in 5 independent experiments. * $p < 0.05$, # $p < 0.01$, analysis of variance by two-tailed unpaired t-test.

Cite this: DOI: 10.1039/c0xx00000x

www.rsc.org/xxxxxx

ARTICLE TYPE

organized into clusters on all kinds of membrane surfaces. To further analyze the different features of inactive EGFR distribution under the three kinds of membranes above, we used Ripley's K function³⁴ to characterize the spatial clustering and diameters of nanoscale domains (see Experimental Section and Fig. S3). Ripley's K function has come into wide application in analyzing super-resolution images of proteins and provided a quantitative measurement of the deviation of the observed distribution from a random distribution^{16,35}. Fig. 1d showed three representative kinds of spatial clustering of inactive EGFR on different membrane surfaces in the form of a linear transformation $L(r)-r$ of Ripley's K function. The positive value of $L(r)-r$ for the tested proteins means cluster formation. The r value corresponding to the maximum of $L(r)-r$, r_{max} , is defined to represent the average cluster diameter in the tested region of $2 \times 2 \mu\text{m}^2$. 60 regions from 10 independent cells were analyzed and obtained nearly the same results. EGFR on the apical surfaces of adherent COS-7 cells tended to form the largest clusters with the average diameter of 240 ± 20 nm and their spatial clustering diameter extended up to 630 ± 30 nm. While EGFR on the basal

surface of adherent COS-7 cells established the smallest r_{max} , only 90 ± 10 nm, and the scope of clustering diameter decreased to 230 ± 20 nm. As for EGFR on the membranes of suspension COS-7 cells, the average cluster diameter was 150 ± 10 nm and the maximum value of r which satisfied clustering was 530 ± 30 nm.

We then analyzed the amount of EGFR clusters (Fig. 1e) and the percentage of EGFR proteins which formed clusters (Fig. 1f). Statistical results showed that these two properties were significantly different among the three conditions. EGFR on the apical surface formed more clusters and $57 \pm 4\%$ of total EGFR participating in clustering. In contrast, there were only a few clusters on the basal surface of cells and the percentage of EGFR proteins assembling into clusters was drastically reduced to $15 \pm 2\%$. For suspension cells, the status of EGFR clustering was between that on the apical surfaces and on the basal surfaces of adherent cells. Some of EGFR generated clusters, and others sporadically distributed in the membranes. The amount of EGFR clusters was slightly greater than that on the basal surface of adherent cells and $30 \pm 2\%$ of EGFR formed clusters.

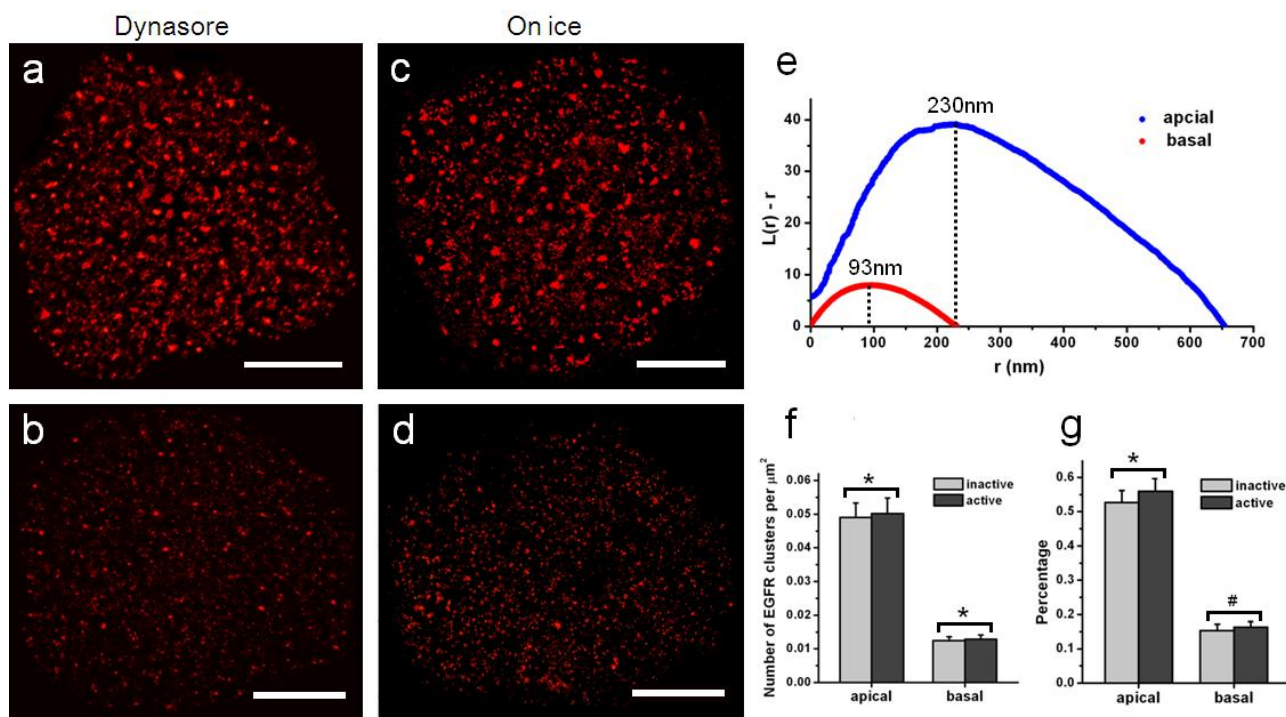


Fig. 2 Active EGFR proteins form clusters with different number and size on different membrane surfaces of COS-7 cells. (a-d) The distribution of active EGFR on the apical (a, c) and basal (b, d) surfaces of adherent COS-7 cells, respectively. In (a) and (b), cells were treated with dynasore to inhibit EGFR endocytosis and then were stimulated with Alexa647-conjugated EGF at 37°C for 5 min. While in (c) and (d), cells were stimulated with Alexa647-conjugated EGF at 37°C for 5 min and then kept on ice for inhibiting EGFR endocytosis during imaging. Scale bars indicate 10 μm . (e) Representative Ripley's K function analysis of EGFR clustering on the apical and basal surfaces of COS-7 cells. The values of r_{max} are 230 nm and 90 nm on the apical and basal surfaces of adherent cells, respectively. 60 regions from 10 cells in 5 independent experiments are analyzed and obtained nearly the same results. (f) Normalized average number of inactive (Cetuximab labeled) and active (EGF labeled) EGFR clusters per μm^2 on the apical and basal membrane surfaces. (g) The percentage of active and inactive EGFR in clusters on the apical and basal membrane surfaces. Data in (f) and (g) are the means \pm standard deviation (s.d.), which were obtained from 10 cell samples in 5 independent experiments. * $p < 0.05$, # $p < 0.01$, analysis of variance by two-tailed unpaired t-test.

Cite this: DOI: 10.1039/c0xx00000x

www.rsc.org/xxxxxx

ARTICLE TYPE

By comparison, we find that EGFR forms clusters with different sizes and numbers in distinct membrane background of the polarized cells. On the apical membrane surfaces of adherent cells, the amount of EGFR clusters is quite high and the average diameter of clusters is big as well, while these parameters decrease dramatically on the basal membrane surfaces. These differences of clustering are potentially caused by various external factors confronted by the two surfaces from polarized cells, such as the levels of cytokines or other signal molecules, as well as the degree of exposure to external environment. The apical membranes of adherent cells are entirely exposed to the external environment and can contact more ligands or signal molecules than the basal membranes. Therefore, inactive EGFR proteins are prone to form more and larger clusters on the apical surfaces of adherent cells so that they can capture more signals and induce dimerization more quickly when stimulated. As for suspension cells, loss of polarity homogenizes the external environment faced by the cells, and the distributions and the functions of the plasma membrane proteins do not recover to the normal growth status, namely the adherent growth. This may be the reason why EGFR on suspension cell membranes can not assemble as many clusters as on the apical surfaces of adherent cells. While suspension cells are entirely immersed into solutions, which lead to the distribution of EGFR isotropous in the whole plasma membrane. Thus EGFR cluster number and the percentage of EGFR forming clusters on suspension cell surfaces were between those values on the apical surfaces and on the basal surfaces of adherent cells.

Visualization the distribution of EGF stimulated EGFR

Since external environments can affect the extent of inactive EGFR clustering, we wonder whether ligands binding could alter the features of clustering. In order to ensure the ligand binding as completely as possible, we tested the effect of a concentration gradient of EGF on the imaging of active EGFR and obtained an optimized labeling efficiency at the concentration of 0.1 $\mu\text{g/ml}$ (Fig. S4). Previous studies have reported that EGF dosage can influence the pathways of activation and internalization³⁶⁻³⁷. Low (1-2 ng/ml) or high (>20 ng/ml) EGF concentration can respectively dictate clathrin-mediated endocytosis (CME) or non-clathrin endocytosis (NCE) including lipid raft-mediated uptake³⁸⁻³⁹. Therefore, 0.1 $\mu\text{g/ml}$ EGF used in our experiments is in the range of concentrations that activates EGFR-NCE.

To observe activated but not internalized EGFR on the membrane surfaces, we treated COS-7 cells with dynasore⁴⁰, a dynamin-2 inhibitor to block EGFR endocytosis. We firstly examined the inhibition of dynasore by three dimensional fluorescent imaging (Fig. S5). The results showed that EGFR internalized or located in the membranes without or with dynasore treatment respectively, indicating the feasibility of this inhibition way. After treated with dynasore, EGFR was stimulated with EGF at 37°C for 5 min and imaged. Fig. 2a and 2b showed the distribution of active EGFR on the apical and

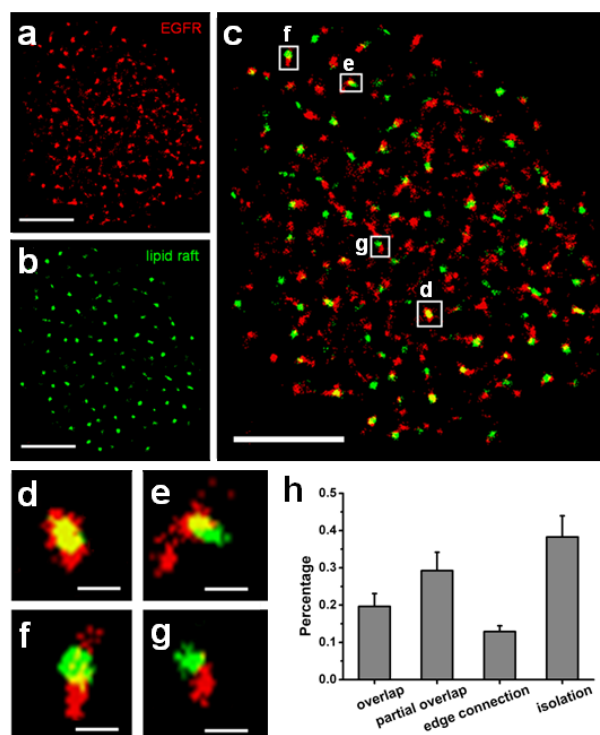


Fig. 3 Inactive EGFR proteins and lipid rafts are significantly colocalized on the apical surfaces of adherent COS-7 cells. (a-b) dSTORM images of Alexa647-conjugated Cetuximab labeled EGFR (a) and Alexa555-conjugated CT-B labeled lipid rafts (b) on the apical surface of the adherent COS-7 cell, respectively. (c) The merging of EGFR (red) and lipid raft (green) channel shows the significant colocalization of the two. (d-g) Magnified view of four representative location relations of EGFR and lipid rafts boxed in (c). From (d) to (g), the location relation is overlap, partial overlap, edge connection and isolation in turn. M_1 and M_2 are 0.72 and 0.98 in (d), 0.61 and 0.37 in (e), 0.18 and 0.15 in (f), 0 and 0.02 in (g). Scale bars indicate 10 μm (a-c), and 200 nm (d-g). (h) The distribution of EGFR and lipid raft spatial association on the apical surfaces of COS-7 cells. About 600 cluster pairs from 5 independent cells are analyzed. Data are the means \pm standard deviation (s.d.).

basal cell membranes. The majority of them still existed in the form of clusters, which was similar to inactive EGFR. As the inhibitors might affect cell morphology, we took the way of keeping the stimulated sample on the ice during imaging to prevent EGFR endocytosis instead of adding inhibitors. Fig. 2c and 2d were the images of active EGFR on the apical and basal membranes. Consistently with inhibitors treating, the results also indicated that active EGFR could form similar clusters as inactive EGFR. Furthermore, from the analysis of Ripley's K function (Fig. 2e) and statistical results (Fig. 2f and 2g), we found that there were no significant differences in cluster number and size between active and inactive EGFR on both apical and basal membranes.

Taken together, the results suggested that innate EGFR proteins have the characteristic of clustering in different environmental conditions, and the clustering is neither caused nor

Cite this: DOI: 10.1039/c0xx00000x

www.rsc.org/xxxxxx

ARTICLE TYPE

changed by EGF stimulation. We reason that the EGFR clusters may serve as the functional unit, which shortens the spatial distances and facilitates EGFR dimerization when ligands bind and magnify signal transduction.

5 The colocalization of EGFR and lipid rafts

The statistical results have showed the average diameter of EGFR clusters was about 200 nm (Fig. 1d), which corresponded with the size of lipid rafts, from 10 nm to 200 nm⁴¹⁻⁴³. Some studies have also indicated that lipid rafts were related to the assembly of protein clusters^{31-32, 44}. Based on this finding, we hypothesized that EGFR clusters would be associated with lipid rafts. We further used dual-color dSTORM imaging to investigate the relationship between the distribution of inactive EGFR and lipid rafts. EGFR proteins were still labeled with Alexa647-conjugated Cetuximab, and lipid rafts were labeled with Alexa555-conjugated cholera toxin subunit B (CT-B), which binds to glycosphingolipids with a strong affinity for GM1, a widely used lipid raft marker⁴⁵. Fig. 3 and Fig. 4 were the representative dSTORM images that displayed the distribution of inactive EGFR and lipid rafts on the apical surface and basal surface of adherent COS-7 cells, respectively. According to Fig. 3b and Fig. 4b, we found that lipid rafts also assembled into many clusters with different sizes. The average cluster diameter of lipid rafts on the apical surfaces of cells ($155 \text{ nm} \pm 30 \text{ nm}$) was larger than that on the basal surfaces ($80 \text{ nm} \pm 20 \text{ nm}$), which had the similar trend with EGFR (Fig. S6). Merged images of lipid rafts and inactive EGFR (Fig. 3c, Fig. 4c) showed a significant colocalization of two types of clusters.

We used Mander's colocalization coefficients⁴⁶ M_1 and M_2 to measure the degrees of spatial association between EGFR and lipid rafts (see Experimental Section). The colocalization coefficients represent the amount of fluorescence of the colocalized area relative to the fluorescence of total area covered by each component. Since the area of EGFR and lipid raft clusters were usually different, M_1 and M_2 were not equal. We classified the distribution of EGFR and lipid rafts into four kinds of locations according to values of M_1 and M_2 . Two types of clusters were defined as overlap if they exhibited an M_1 or M_2 greater than 0.66. The cluster pairs with both M_1 and M_2 less than 0.33 but more than zero were defined as edge connection. The cluster pairs in which M_1 or M_2 equaled to zero were characterized as isolation. The rest of cluster pairs were classified as partial overlap. Magnified boxed images of Fig. 3c and Fig. 4c showed the four localization statuses on the apical (Fig. 3d-g) and basal (Fig. 4d-g) cell surfaces in detail, respectively. Statistical analysis of multiple images by measurement of Mander's colocalization coefficients showed the percentage of the four kinds of locations on the apical (Fig. 3h) and basal (Fig. 4h) cell surfaces. The spatial association of overlap and partial overlap was collectively referred to as colocalization. The results revealed that $50 \pm 6\%$ of EGFR colocalized with lipid rafts on the apical

surfaces of COS-7 cells, and the colocalization percentage ($51 \pm 7\%$) did not change evidently on the basal surfaces.

The acquisition time of two channels in sequence (less than 8 min), which is longer than that of a single channel, may cause larger sample drift owing to the mobility of cell membranes. Therefore, dual-color dSTORM imaging of EGFR and lipid rafts was also performed on fixed cell membranes as controls (Figure S7). The results showed that the distribution and colocalization of EGFR and lipid rafts had no significant differences between live and fixed cell membranes, suggesting that cell membranes did not move obviously during this short time under STORM imaging conditions and the drift could be corrected by TetraSpeck microspheres (see Experimental Section).

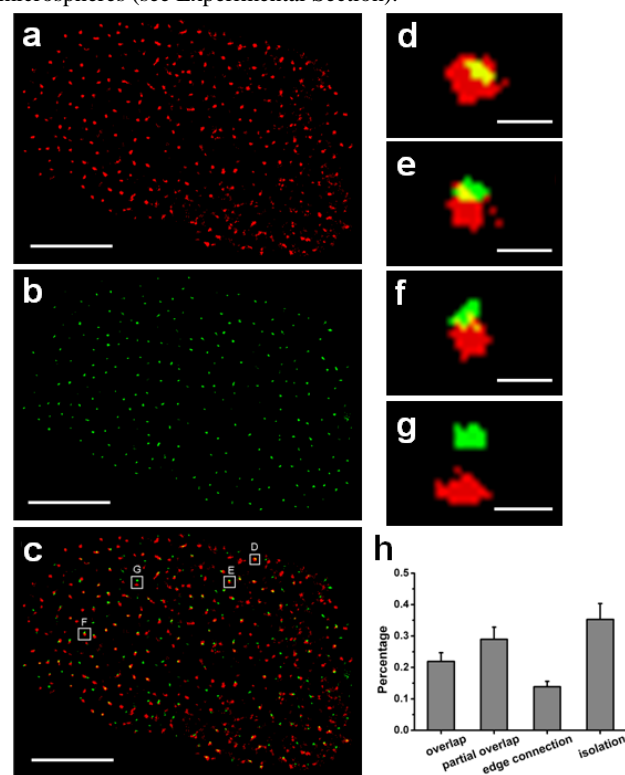


Fig. 4 Inactive EGFR proteins and lipid rafts are mainly colocalized on the basal surfaces of adherent COS-7 cells. (a-b) dSTORM images of Alexa647-conjugated Cetuximab labeled EGFR (a) and Alexa555-conjugated CT-B labeled lipid rafts (b) on the basal surface of the adherent COS-7 cell, respectively. (c) The merging of EGFR (red) and lipid raft (green) channel shows the significant colocalization of the two. (d-g) Magnified view of four representative location relations of EGFR and lipid rafts boxed in (c). From (d) to (g), the location relation is overlap, partial overlap, edge connection and isolation in turn. M_1 and M_2 are 0.41 and 1 in (d), 0.19 and 0.35 in (e), 0.05 and 0.06 in (f), and both zero in (g). Scale bars indicate $10 \mu\text{m}$ (a-c), and 200 nm (d-g). (h) The distribution of EGFR and lipid raft spatial association on the basal surfaces of COS-7 cells. About 600 cluster pairs from 5 independent cells are analyzed. Data are the means \pm standard deviation (s.d.).

In addition, active EGFR labeled with EGF were also used to detect the colocalization with lipid rafts (Fig. S8). We obtained

almost the same results: there were $49 \pm 5\%$ and $47 \pm 6\%$ of active EGFR colocalized with lipid rafts on the apical and basal surfaces of cells, respectively.

5 The disruption of lipid rafts weakens EGFR clustering

To further verify whether EGFR proteins were associated with lipid rafts, COS-7 cells labeled with Alexa647-conjugated Cetuximab were treated with 10 mM methyl- β -cyclodextrin (M β CD) at the room temperature for 20-30 min to extract membrane cholesterol, which was an important component of lipid rafts. Fig. 5a-d showed the significant changes in the distribution of inactive EGFR on the apical and basal surfaces of cells before and after treating with M β CD. We found that a number of EGFR clusters had become smaller or even disappeared after cholesterol depletion. Analysis of the degree of EGFR clustering by Ripley's K function as above mentioned revealed that clustering range became narrow which decreased from 640 nm to 160 nm on the apical membranes and from 240 nm to 80 nm on the basal membranes (Fig. 5e and 5f). The average diameter of EGFR clusters dropped from 240 nm to 80 nm on the apical surfaces, and the plot even continued to decline

on the basal surface which meant EGFR hardly form clusters after adding M β CD (Fig. 5e and 5f). Considerable reduction was also exhibited in cluster number after treating with M β CD (Fig. 5g and 5h). When using Alexa647-conjugated EGF to stimulate EGFR, we observed that the active EGFR had the similar phenomenon of clusters decreasing after adding M β CD (Fig. S9).

Dual color imaging of EGFR and lipid rafts, together with the disruption of lipid rafts by extracting cholesterol, demonstrate that lipid rafts contribute to the formation of EGFR clusters. The distributions of EGFR and lipid rafts both have the characteristic of clustering, especially on the apical surfaces of adherent COS-7 cells, and the majority of them are significantly colocalized with each other. After using M β CD to disrupt the structure of lipid rafts, EGFR clusters decrease dramatically or even disappear, and the distribution of EGFR become sporadic in the whole membrane. The reduction of the amount and size of EGFR clusters may be due to partial or complete fragmentation of larger EGFR clusters coupling with the destruction of lipid rafts. Furthermore, the relationship of localization between EGFR clusters and lipid rafts does not change no matter what status these EGFR proteins are.

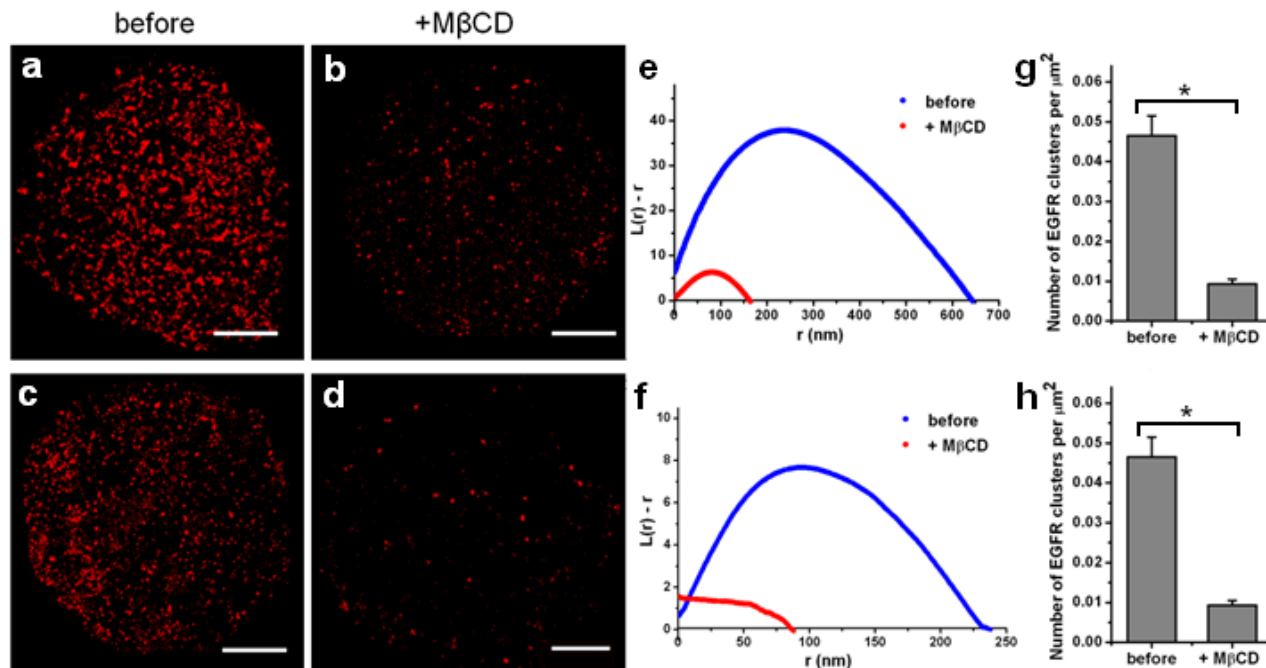


Fig.5 M β CD treatment disrupts the EGFR clustering on both apical and basal membrane surfaces of COS-7 cells. (a-b) dSTORM images of EGFR on the apical surface of the adherent COS-7 cell before (a) and after (b) treating with M β CD. (c-d) Changes of the distribution of EGFR on the basal membrane surface as (a) and (b). EGFR was labeled with Alexa647-conjugated Cetuximab. Scale bars indicate 10 μm (a-d). (e-f) Representative Ripley's K function analysis of EGFR clustering on the apical (e) and basal (f) membrane surfaces before and after treating with M β CD. The value of r_{max} decreases from 240 nm to 80 nm after treating with M β CD on the apical surface, and the value of $L(r) - r$ even continues to decline on the basal surfaces which means EGFR hardly form clusters. 60 regions from 10 cells in 5 independent experiments are analyzed and obtained nearly the same results. (g-h) Normalized number of EGFR clusters per μm^2 before and after adding M β CD on the apical (g) and basal (h) membrane surfaces. Data are the means \pm standard deviation (s.d.), which were obtained from 10 cell samples in 5 independent experiments. * $p < 0.05$, analysis of variance by two-tailed unpaired t-test.

Conclusions

In summary, our results uncover the properties of EGFR clustering distribution in different membrane environments, which suggests the cell polarity-dependent distribution pattern of EGFR proteins --- more and larger clusters on the apical membrane surfaces than on the basal membrane surfaces, and

illustrates the contribution of lipid rafts to EGFR cluster formation. As for the clustering process, our work here not only puts an emphasis on the heterogeneous distribution associated with cell polarity, but also finds a key factor --- lipid rafts that mediate the unique EGFR distribution pattern. The two causes indicate that the clustering process of membrane receptors relies on various aspects, including the membrane sub-area they are

located, the membrane sub-domains they contact, and even the surrounding niches.

This work paves the way to further quantitatively study the distribution of EGFR molecules within each cluster and investigate a clear relation of cluster size and the extent of signal transduction. Meanwhile, understanding the distribution of EGFR on the membranes of living cells and some factors that affect EGFR clustering can also provide a basis for development of therapeutic drugs against tumors.

10 Experimental section

Labeling ligands

Cetuximab (Merck) or EGF (Sigma-Aldrich) was labeled with Alexa647 (Invitrogen) in an appropriate concentration. 0.2 μ l Alexa647 (1 mg/ml, dissolved in DMSO) was added in 100 μ l Cetuximab or EGF (100 μ g/ml, dissolved in PBS) and vortexed in dark for 2 hours at room temperature to react completely. Then the mixture was filtered by illustra NAP-5 columns (GE Healthcare) to remove excessive dyes and collected the eluant. The A650 and A280 was read to determine in which tube(s) the labeling ratio of Alexa647 and Cetuximab or EGF was 0.7~1 dye/protein by absorption spectroscopy assay. Fractions meeting this criterion were pooled for use.

Cell culture

COS-7 cells were cultured in Dulbecco's modified Eagle's medium (Hyclone) with 10% fetal bovine serum (FBS) (Biochrom AG, Germany) and antibiotics (100 U/ml streptomycin and 100 μ g/ml penicillin) (Invitrogen, USA) at 37°C in a humidified atmosphere with 5% CO₂.

Sample preparation

The day before the experiment, cells were detached with trypsin/EDTA. They were plated on pre-cleaned coverslips and cultured in serum free condition for 24 hours. For inactive EGFR imaging, cells were washed three times with PBS and blocked by incubating in 1% BSA for 30 min. After washing out the blocking buffer by PBS for three times, the sample was stained with 50 μ l Alexa647- conjugated Cetuximab and incubated in dark for 10 min at 4°C. Finally the sample was washed by PBS for three times.

For active EGFR imaging, cells were treated with 80 μ M dynasore (Sigma-Aldrich) for 30 min to inhibit EGFR endocytosis and washed by PBS containing 1% BSA for three times. Then cells were stained by 0.1 μ g/ml Alexa647-conjugated EGF in dark for 5 min at 37°C to stimulate EGFR. After that, the sample was washed by PBS for three times. Another way to prepare active EGFR sample was also applied. Similarly, cells were added Alexa647-conjugated EGF to stimulate EGFR at 37°C for 5 min but not treated with inhibitors, and then washed out the staining solution. The sample was kept on ice all the time during imaging.

For suspension cell imaging, new produced cell suspension was stained with Alexa647- conjugated Cetuximab in dark for 10 min at 4°C and centrifuged at 1000 rpm for 5 min to eliminate staining solution. Cells were resuspended with PBS and centrifuged at 1000 rpm for 5 min. After repeating 2 times, the

suspension cells were placed on the glass slides and kept for 20 min to adhesion.

For dual-color imaging of living cells, cells were treated as stated above except labeled with two staining solutions at the same time, Alexa647-conjugated Cetuximab/EGF and Alexa555-conjugated CT-B (Invitrogen). For fixed samples, cells were treated with 4% paraformaldehyde in dark for 10 min, washed by PBS for 3 times and stained with Alexa647-conjugated Cetuximab prior to imaging.

Before sealing the sample, imaging buffer was added which contained no phenol red DMEM, 1 M HEPES (pH 8.0), 50% (w/v) glucose, 0.5 mg/ml glucose oxidase (Sigma-Aldrich), 40 μ g/ml catalase (Sigma-Aldrich) and 0.5% (v/v) mercaptoethylamine.

Microscope setup and imaging

dSTORM imaging was performed on a Nikon Ti-E microscope with a 100 \times 1.49 NA TIRF lens (Nikon, Japan) using a 561 nm laser (200 mw) and 640 nm laser (100 mw). For single-color dSTORM imaging of EGFR, the sample was excited by 640 nm laser only. For dual-color dSTORM, the sample was first excited by 640 nm laser for obtaining EGFR imaging and then photoactivated by 561 nm laser power for obtaining lipid raft imaging. The system was equipped with one dichroic filter which reflects both 561 nm and 647 nm laser and imaged on an EMCCD camera (Photometrics, Cascade II). A time series of 5000 frames per cell were recorded at rate of 25 Hz for the reconstruction of the super-resolution imaging. Obtaining one single or dual color dSTORM imaging usually took less than 8 minutes. During this short acquisition time, the z-drift was eliminated by a focus lock, and 100 nm diameter of TetraSpeck microspheres (Invitrogen) were embedded as fiducial markers to correct the x-y drift of the sample and the optical registration between Alexa647 and Alexa555 channels for dual color imaging.

For imaging data analyses, a freely available plug-in for Image J named quickPALM⁴⁷ was applied to analyze raw images⁴⁸. Image TIFF stacks were first pre-processed via background subtraction. For each frame, particles corresponding to single photoemission events were identified with a minimum SNR of 2–4. Then fluorescence peaks were identified in each frame and fitted a least-squares fit with an elliptical Gaussian function. Individual least-squares fit estimates were performed by a threshold of the peak height and the peak widths in the two lateral dimensions. After rejecting the poor fit and asymmetric PSFs, the centroid positions of peaks were determined. STORM images were reconstructed using the precise localization data of single fluorescent molecules obtained from the fits.

Cluster analysis

To analyze EGFR spatial distribution in the plasma membrane, Ripley's K function^{34, 49-50} was used to analyze the cluster characteristic on the localization data established as described above. The examined region of 2 \times 2 μ m² in the reconstructed images was selected. Ripley's K-function was then calculated as:

Where A is the image area, N is the number of total localizations in the area, r is the spatial scale (radius) for the K -function calculation and δ_{ij} is the distance between points the i -th and the j -th localizations. Here, if δ_{ij} is less than r , the value will be one, otherwise $\delta_{ij} = 0$. This essentially counts the number of other points encircled by concentric rings centered on each point. The linear transformation of $K(r)$ was used to interpret the spatial randomness:

The amplitude of $L(r)-r$ would be zero for particles with a random distribution, and positive for clustering particles. Edge-effects were negated by weighting edge points and cropping image edges after the calculation. The values of $L(r)$ generated by each particle were used to produce a cluster map by interpolating a surface plot with $L(r)$ as the z-axis. Then a binary cluster map was generated through a defined $L(r)$ threshold. For example, the percentage of points which satisfied $L(r)-r > 0$ is 60%, and the $L(r)$ threshold was set at 40% of the maximum value of $L(r)$ from the plot. Finally the information of clustering could be extracted from the binary map, such as the number and the size of clusters. The percentage of EGFR in clusters was calculated via dividing the number of points which satisfied $L(r)-r > 0$ by the total number of points in the region. All the statistical data of cluster properties were derived from 60 regions of 10 cell samples in 5 independent experiments. All calculations and image processing were performed in Matlab.

Colocalization analysis

To quantify the spatial association of EGFR and lipid raft clusters, a dual-color dSTORM image with zero background intensity was used to compute Mander's colocalization coefficients⁴⁶ M_1 and M_2 via Image-Pro Plus. The cluster pairs with M_1 or M_2 equal to zero were classified as isolated clusters. When both M_1 and M_2 were less than 0.33 but larger than zero, the cluster pairs were assigned to the edge-connected category. The highly overlapping category was defined as M_1 or M_2 greater than 0.66. The rest of the cluster pairs belonged to the partially overlapping category.

Acknowledgements

This work was financially supported by MOST (Grant No. 2011CB933600), NSFC (Grant No. 21373200).

Notes and references

^aState Key Laboratory of Electroanalytical Chemistry, Changchun Institute of Applied Chemistry, Chinese Academy of Sciences, Changchun, Jilin 130022, P.R. China. Fax: +86 431 85262684; Tel: +86 431 85262684; E-mail: hongdawang@ciac.ac.cn

^bState Key laboratory of Cell Biology, Institute of Biochemistry and Cell Biology, Shanghai Institutes for Biological Sciences, Chinese Academy of Sciences, Shanghai 200031, P.R. China. Fax: +86 21 54921107; Tel: +86 21 54921107; E-mail: hbji@sibcb.ac.cn

^cGraduate University of Chinese Academy of Sciences, Beijing 100049, P.R. China.

† Electronic Supplementary Information (ESI) available. See DOI: 10.1039/b000000x/

1. K. Simons and E. Ikonen, *Nature*, 1997, **387**, 569-572.

2. K. Jacobson, E. D. Sheets and R. Simson, *Science*, 1995, **268**, 1441-1442.
3. S. R. Shaikh, A. C. Dumaul, L. J. Jencki and W. Stillwell, *Biochimica Et Biophysica Acta-Biomembranes*, 2001, **1512**, 317-328.
4. G. Vereb, J. Matko, G. Vamosi, S. M. Ibrahim, E. Magyar, S. Varga, J. Szollosi, A. Jenei, R. Gaspar, T. A. Waldmann and S. Damjanovich, *Proceedings of the National Academy of Sciences of the United States of America*, 2000, **97**, 6013-6018.
5. M. J. Rust, M. Bates and X. Zhuang, *Nature Methods*, 2006, **3**, 793-795.
6. D. Kamiyama and B. Huang, *Developmental Cell*, 2012, **23**, 1103-1110.
7. M. Heilemann, S. van de Linde, A. Mukherjee and M. Sauer, *Angewandte Chemie-International Edition*, 2009, **48**, 6903-6908.
8. E. Betzig, G. H. Patterson, R. Sougrat, O. W. Lindwasser, S. Olenych, J. S. Bonifacino, M. W. Davidson, J. Lippincott-Schwartz and H. F. Hess, *Science*, 2006, **313**, 1642-1645.
9. T. J. Gould, V. V. Verkhusha and S. T. Hess, *Nature Protocols*, 2009, **4**, 291-308.
10. C. Kukat, C. A. Wurm, H. Spahr, M. Falkenberg, N. G. Larsson and S. Jakobs, *Proceedings of the National Academy of Sciences of the United States of America*, 2011, **108**, 13534-13539.
11. S. van de Linde, S. Aufmkolk, C. Franke, T. Holm, T. Klein, A. Loeschberger, S. Proppert, S. Wolter and M. Sauer, *Chemistry & Biology*, 2013, **20**, 8-18.
12. P. Sengupta, S. B. van Engelenburg and J. Lippincott-Schwartz, *Chemical Reviews*, 2014, **114**, 3189-3202.
13. D. Goswami, K. Gowrishankar, S. Bilgrami, S. Ghosh, R. Raghupathy, R. Chadda, R. Vishwakarma, M. Rao and S. Mayor, *Cell*, 2008, **135**, 1085-1097.
14. B. F. Lillemeier, M. A. Moertelmaier, M. B. Forstner, J. B. Huppa, J. T. Groves and M. M. Davis, *Nature Immunology*, 2010, **11**, 90-U106.
15. P. Sengupta, T. Jovanovic-Taliman, D. Skoko, M. Renz, S. L. Veatch and J. Lippincott-Schwartz, *Nature Methods*, 2011, **8**, 969-975.
16. J. S. Aaron, B. D. Carson and J. A. Timlin, *Small*, 2012, **8**, 3041-3049.
17. T. Lang and S. O. Rizzoli, *Physiology*, 2010, **25**, 116-124.
18. A. Citri and Y. Yarden, *Nature Reviews Molecular Cell Biology*, 2006, **7**, 505-516.
19. R. N. Jorissen, F. Walker, N. Pouliot, T. P. J. Garrett, C. W. Ward and A. W. Burgess, *Experimental Cell Research*, 2003, **284**, 31-53.
20. P. Klein, D. Mattoon, M. A. Lemmon and J. Schlessinger, *Proceedings of the National Academy of Sciences of the United States of America*, 2004, **101**, 929-934.
21. A. De Luca, A. Carotenuto, A. Rachiglio, M. Gallo, M. R. Maiello, D. Aldinucci, A. Pinto and N. Normanno, *Journal of Cellular Physiology*, 2008, **214**, 559-567.
22. K. M. Ferguson, in *Annual Review of Biophysics*, 2008, vol. 37, pp. 353-373.
23. E. G. Hofman, A. N. Bader, J. Voortman, D. J. van den Heuvel, S. Sigismund, A. J. Verkleij, H. C. Gerritsen and P. M. P. v. B. E. Henegouwen, *Journal of Biological Chemistry*, 2010, **285**, 39481-39489.
24. M. A. Lemmon and J. Schlessinger, *Cell*, 2010, **141**, 1117-1134.
25. A. Abulrob, Z. Lu, E. Baumann, D. Vobornik, R. Taylor, D. Stanimirovic and L. J. Johnston, *Journal of Biological Chemistry*, 2010, **285**, 3145-3156.
26. Y. Wang, J. Gao, X. Guo, T. Tong, X. Shi, L. Li, M. Qi, Y. Wang, M. Cai, J. Jiang, C. Xu, H. Ji and H. Wang, *Cell Research*, 2014, **24**, 959-976.
27. K. M. Ferguson, M. B. Berger, J. M. Mendrola, H. S. Cho, D. J. Leahy and M. A. Lemmon, *Molecular Cell*, 2003, **11**, 507-517.
28. N. Jura, N. F. Endres, K. Engel, S. Deindl, R. Das, M. H. Lamers, D. E. Wemmer, X. Zhang and J. Kuriyan, *Cell*, 2009, **137**, 1293-1307.
29. X. Zhang, J. Gureasko, K. Shen, P. A. Cole and J. Kuriyan, *Cell*, 2006, **125**, 1137-1149.
30. H. Mizuno, M. Abe, P. Dedecker, A. Makino, S. Rocha, Y. Ohno-Iwashita, J. Hofkens, T. Kobayashi and A. Miyawaki, *Chemical Science*, 2011, **2**, 1548-1553.

-
31. D. M. Owen, A. Magenau, D. Williamson and K. Gaus, *Bioessays*, 2012, **34**, 739-747.
32. S. M. Pontier, Y. Percherancier, S. Galandrin, A. Breit, C. Gales and M. Bouvier, *Journal of Biological Chemistry*, 2008, **283**, 24659-24672.
- 5 33. W. A. Messersmith and D. J. Ahnen, *New England Journal of Medicine*, 2008, **359**, 1834-1836.
34. D. M. Owen, C. Rentero, J. Rossy, A. Magenau, D. Williamson, M. Rodriguez and K. Gaus, *Journal of Biophotonics*, 2008, **3**, 446-454.
- 10 35. M. Lehmann, S. Rocha, B. Mangeat, F. Blanchet, H. Uji-i, J. Hofkens and V. Pigué, *Plos Pathogens*, 2011, **7**.
36. S. Polo, P. P. Di Fiore and S. Sigismund, *Cell Cycle*, 2014, **13**, 681-682.
37. S. Sigismund, V. Algisi, G. Nappo, A. Conte, R. Pascolutti, A. Cuomo, T. Bonaldi, E. Argenzio, L. G. G. C. Verhoef, E. Maspero, F. Bianchi, F. Capuani, A. Ciliberto, S. Polo and P. P. Di Fiore, *Embo Journal*, 2013, **32**, 2140-2157.
- 15 38. S. Sigismund, E. Argenzio, D. Tosoni, E. Cavallaro, S. Polo and P. P. Di Fiore, *Developmental Cell*, 2008, **15**, 209-219.
- 20 39. S. Sigismund, T. Woelk, C. Puri, E. Maspero, C. Tacchetti, P. Transidico, P. P. Di Fiore and S. Polo, *Proceedings of the National Academy of Sciences of the United States of America*, 2005, **102**, 2760-2765.
40. E. Macia, M. Ehrlich, R. Massol, E. Boucrot, C. Brunner and T. Kirchhausen, *Developmental Cell*, 2006, **10**, 839-850.
- 25 41. D. V. Nicolau, K. Burrage, R. G. Parton and J. F. Hancock, *Molecular and Cellular Biology*, 2006, **26**, 313-323.
42. L. J. Pike, *Journal of Lipid Research*, 2006, **47**, 1597-1598.
43. M. Cai, W. Zhao, X. Shang, J. Jiang, H. Ji, Z. Tang and H. Wang, *Small*, 2012, **8**, 1243-1250.
- 30 44. S. K. Patra, *Biochimica Et Biophysica Acta-Reviews on Cancer*, 2008, **1785**, 182-206.
45. P. W. Janes, S. C. Ley and A. I. Magee, *Journal of Cell Biology*, 1999, **147**, 447-461.
- 35 46. E. M. M. Manders, F. J. Verbeek and J. A. Aten, *Journal of Microscopy-Oxford*, 1993, **169**, 375-382.
47. R. Henriques, M. Lelek, E. F. Fornasiero, F. Valtorta, C. Zimmer and M. M. Mhlanga, *Nature Methods*, 2010, **7**, 339-340.
48. S. Wolter, M. Schuettpehl, M. Tscherepanow, S. Van de Linde, M. Heilemann and M. Sauer, *Journal of Microscopy-Oxford*, 2009, **237**, 12-22.
- 40 49. B. D. Ripley, *Journal of the Royal Statistical Society Series B-Methodological*, 1979, **41**, 368-374.
50. A. L. McEvoy, D. Greenfield, M. Bates and J. Liphardt, *Bmc Biology*, 2010, **8**.
- 45